ACS APPLIED MATERIALS & INTERFACES

Research Article

www.acsami.org

New Ruthenium Sensitizers Featuring Bulky Ancillary Ligands Combined with a Dual Functioned Coadsorbent for High Efficiency Dye-Sensitized Solar Cells

Yongbo Shi, Mao Liang,* Lina Wang, Hongyu Han, Lingshan You, Zhe Sun, and Song Xue*

Department of Applied Chemistry, Tianjin University of Technology, Tianjin, 300384, P.R.China

Supporting Information

ABSTRACT: Two ruthenium complexes featuring bulky ancillary ligands, XS48 and XS49, were synthesized and studied as dyes in dye-sensitized solar cells (DSCs). Both dyes exhibit higher solar-to-electrical energy conversion efficiency when compared to a commonly used N3 sensitizer under the same conditions. To examine the influence of the bulky ancillary ligands and alleviate the electron recombination in cells, we have developed a dual functioned truxene-based coadsorbent (MXD1) as an alternative candidate to chenodeoxycholic acid (CDCA). This coadsorbent not only effectively shields the back electron transfer from the TiO_2 to I_3^- ions but also enhances the light harvesting ability in the short wavelength regions. The photovoltaic performance of XS48-sensitized DSC was independent of the coadsorbents, while XS49 with large bulky ancillary ligand presented better performance when coadsorbent was employed. Interestingly, the simultaneous adsorption-to-sequential adsorption of XS48/49 and MXD1 has caused a notably improved photovoltage, which can be primarily ascribed to the enhanced dye adsorption and retardation of charge recombination. These results not only provide a new vision on how ancillary ligands affect the performance of ruthenium complexes but also open up a new way to achieve further efficiency enhancement of ruthenium complexes.

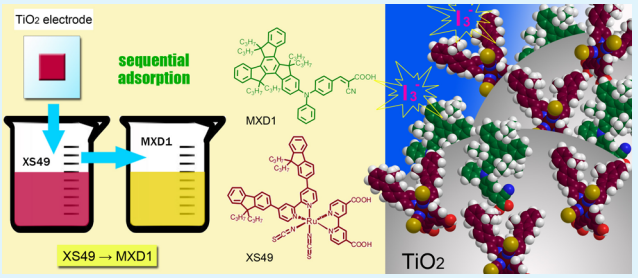

KEYWORDS: *ruthenium complexes, extinction coefficients, ancillary ligand, charge recombination, coadsorbent, sequential adsorption*

INTRODUCTION

Dye-sensitized solar cells (DSCs), as a new type of photovoltaic technology, have been considered to be a credible alternative to conventional inorganic silicon-based solar cells because of their ease of fabrication, high efficiency, and cost-effectiveness since the report by O'Regan and Grätzel.[1] To achieve high solar power conversion efficiency, many efforts have been dedicated to the design and synthesis of ruthenium(II) complexes,[2−32] zinc porphyrin complexes,[33] and metal free organic dyes.[34−36] Typically, ruthenium(II) complexes had a central role in significantly advancing the DSC technology due to their remarkable performance.

The prominent feature of ruthenium dyes is their broad absorptivity from the visible to the near-infrared (NIR) region because of metal-to-ligand charge transfer (MLCT) characteristics. However, the molar extinction coefficients of these dyes are moderate for the long wavelength. Fortunately, this problem can be alleviated by the increasing conjugation on the ancillary bipyridine ligand through the incorporation of electron-rich benzenoid cores[11−17] or heteroaromatic rings[18−32] as donor end-substituents. As demonstrated in the literature, this strategy is quite successful, and good results have been obtained. For example, power conversion efficiencies of 11.7−12.1% were achieved by C106 at the AM1.5G conditions.[25]

Besides the extinction coefficient, there are two crucial factors that affect the performance of DSCs, namely, the formation of molecular aggregates[30,37] on the surface of the TiO_2 nanocrystalline film and the charge recombination[37] between electrons at the TiO_2 and I_3^- ions. A survey of the literature revealed that most ruthenium dyes required the presence of coadsorbents (e.g., chenodeoxycholic acid (CDCA)) that minimized the formation of molecular aggregates[13,25] on the surface of the TiO_2 nanocrystalline film and reduced the charge recombination in cells. Actually, an introduction of ancillary ligands with expansion of the π-conjugated system in ruthenium sensitizers not only enhances the molar extinction coefficients but also induces unexpected dye packing. These ancillary ligands have a dramatic influence on the dye aggregation and charge recombination and, hence, the cell performance.

To enhance the molar extinction coefficient of ruthenium dyes and study the effect of the bulky ancillary ligands on the performance of the dyes, we have developed two ruthenium dyes (XS48 and XS49, Figure 1) that contain butyloxy-substituted benzene ring and 9,9-dipropyl-9*H*-fluorene on the ancillary bipyridine ligand, respectively. Both the bulky groups possess electron-rich nature and good stability. The influences of the ancillary ligands upon the photophysical, photochemical, and electrochemical properties and photovoltaic performances were investigated. Furthermore, in order to reduce the possible molecular aggregate

Received: October 14, 2012
Accepted: December 12, 2012
Published: December 12, 2012

   dx.doi.org/10.1021/am302318z | ACS Appl. Mater. Interfaces 2013, 5, 144−153

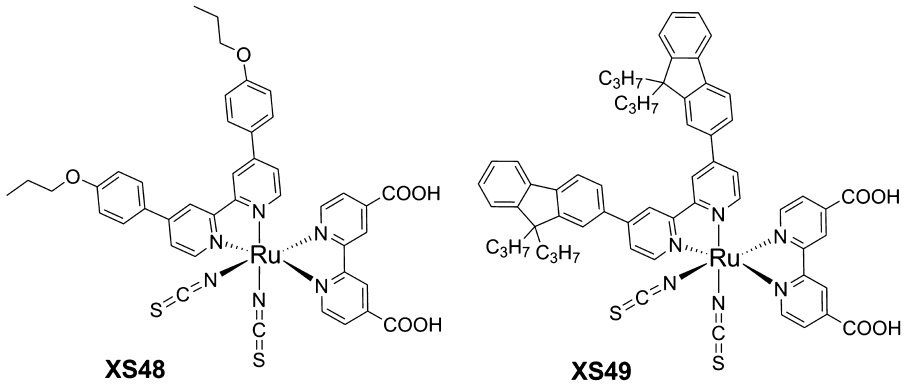

Figure 1. Molecular structures of dyes.

Scheme 1. Synthetic Routes for Dyes XS48 and XS49

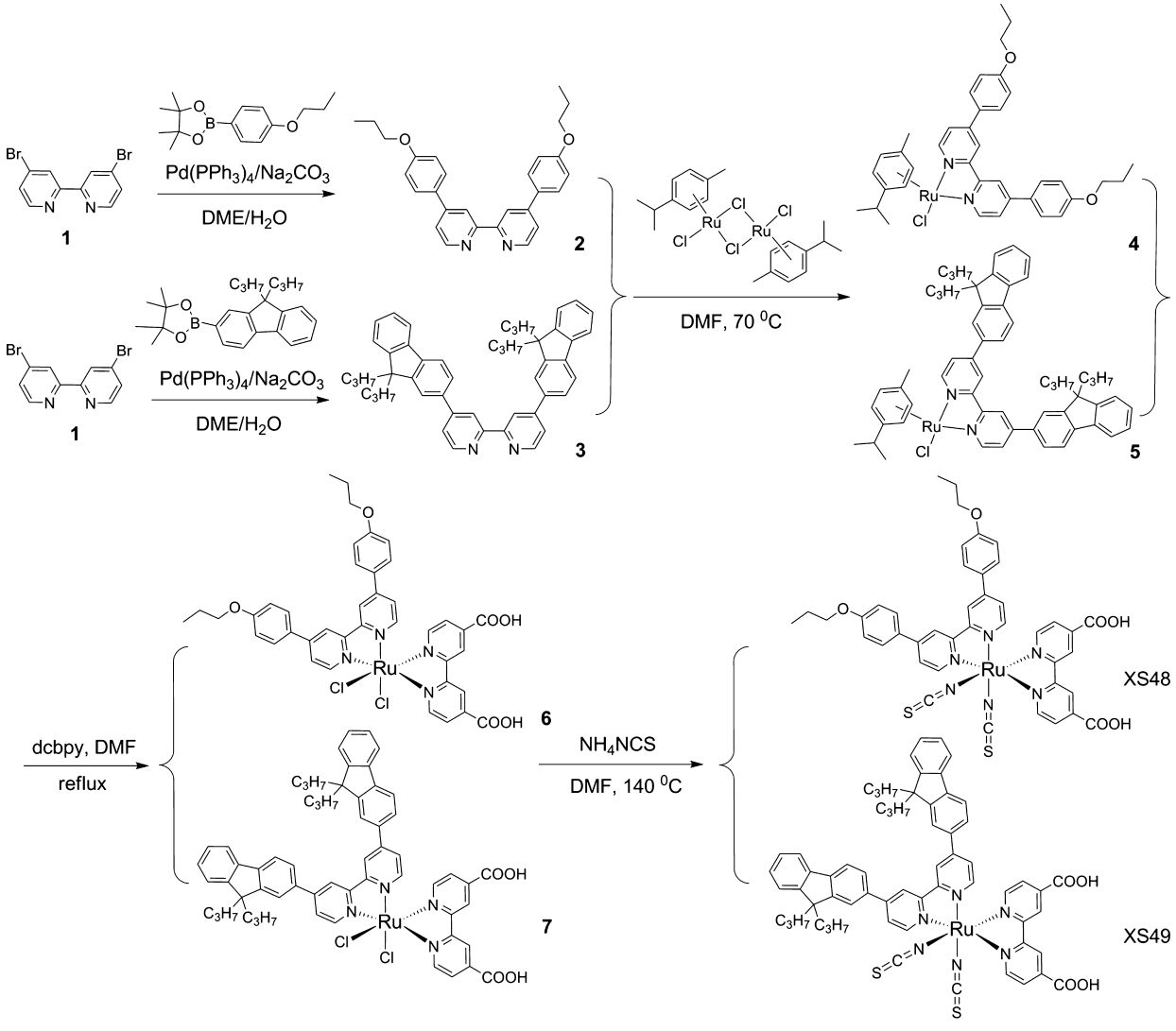

and charge recombination pathway occurring at the TiO_2/dye/electrolyte interface, a truxene-based triarylamine dye has been introduced as coadsorbents onto the TiO_2 surface. Our results highlight the strategy of incorporation of electron-rich benzenoid cores in the ancillary ligands for improving the performance of the ruthenium dyes. Particularly, the superiority of employing sequential adsorption relative to simultaneous adsorption is observed when bulky coadsorbent is introduced for DSCs.

EXPERIMENTAL SECTION

Materials and Methods. The synthetic routes for dyes XS48 and XS49 were shown in Scheme 1. Titanium(IV) isopropoxide, tertbutylpyridine, and lithium iodide were purchased from Aldrich. All other solvents and chemicals used in this work were analytical grade and used without further purification.

Melting points of the samples were taken on an RY-1 melting point apparatus (Tianfen, China). ^{1}H NMR and ^{13}C NMR spectra were

dx.doi.org/10.1021/am302318z | ACS Appl. Mater. Interfaces 2013, 5, 144−153

recorded on a Bruker AM-400 spectrometer. The reported chemical shifts were against TMS. High resolution mass spectra were obtained with a Micromass GCT−TOF mass spectrometer.

Synthesis of 4-(4-Propoxyphexyl)-2-(4-(4-propoxyphenyl)-pyridin-2-yl) pyridine (2). 4,4,5,5-Tetramethyl-2-(4-propoxyphenyl)-1,3,2-dioxaborolane (1.0 g, 3.8 mmol), 4,4′-dibromo-2,2′-bipyridyl (1.0 g, 3.2 mmol), $Pd(PPh_3)_4$ (5 mol %), and K_2CO_3 (9.2 g, 6.7 mmol) were dissolved in 1,2-dimethoxyethane (DME, 15 mL)/H_2O (3 mL) and refluxed overnight. H_2O and ethyl acetate were added; the extract was washed with brine, dried with anhydrous $MgSO_4$. The solvent was evaporated, and the remaining crude product was purified by column chromatography to give a white crystal of **2**. Yield: 43.9%. Mp: 270−272 °C; IR (KBr): 2962, 2936, 2876, 1607, 1518, 1455, 1286, 1241, 1187 cm^{-1}; ^1H NMR (400 MHz, $CDCl_3$): δ 8.72−8.69 (m, 4H), 7.78−7.73 (m, 4H), 7.55−7.51 (d, J = 4.7 Hz, 2H), 7.02 (d, J = 8.3 Hz, 4H), 3.99 (t, J = 6.6 Hz, 4H), 1.90−1.80 (m, 4H), 1.10−1.04 (m, 6H); ^{13}C NMR (100 MHz, $CDCl_3$): δ 160.2, 156.3, 149.4, 149.1, 130.2, 128.4, 121.1, 118.7, 115.0, 69.7, 22.6, 10.5.

Synthesis of cis-bis(Thiocyanato)(2,2′-bipyridyl-4,4′-dicarboxylato){4,4′-bis(4-propoxyphenyl)-2,2′-bipyridine}-ruthenium(II) (XS48). A flask protected by nitrogen flushing was charged with a solution of **2** (296.9 mg, 0.7 mmol) and a dichloro-(*p*-cymene)ruthenium(II) dimer (216.5 mg, 0.2 mmol) in *N*,*N*-dimethylformamide (DMF, 15 mL). The mixture was stirred at 70 °C for 4 h under reduced light. Subsequently, 4,4′-dicarboxyl-2,2′-bipyridine (172.7 mg, 0.71 mmol) was added into the flask. The reaction mixture was refluxed for 4 h. An excess of NH_4NCS (537.5 mg, 7.1 mmol) was added to the resulting dark solution, and the reaction continued to reflux for another 4 h. After that, the reaction mixture was cooled down to room temperature, and the solvent was removed under vacuum. H_2O was added to induce the precipitate. The resulting solid was filtered and washed with H_2O and dried under vacuum. The resulting solid was dissolved in methanol (CH_3OH) which contained 2.5 equiv of tetrabutylammonium hydroxide solution and purified on a Sephadex LH-20 column with CH_3OH as the eluent. The collected main band was concentrated, and the solution pH was lowered to 4.8 using 0.02 M nitric acid. The precipitate was collected on a sintered glass crucible by suction filtration and dried in air. Yield: 46.1%. IR (KBr): 3402, 2958, 2875, 2106, 1601, 1470, 1377, 1251, 1182 cm^{-1}. ^1H NMR (DMSO-d_6, 300 MHz) δ: 9.32−8.81 (m, 6H), 8.32−8.12 (m, 4H), 7.89 (m, 2H), 7.81−7.38 (m, 4H), 7.20 (d, J = 8.7 Hz, 2H), 7.06 (dd, J = 8.7, 2.4 Hz, 2H), 4.08 (t, J = 6.6 Hz, 2H), 3.99 (t, J = 6.6 Hz, 2H), 1.79 (m, 4H), 1.03 (t, J = 7.2 Hz, 6H); ^{13}C NMR (DMSO-d_6, 300 MHz) δ: 163.5, 162.9, 159.2, 159.0, 157.5, 156.2, 151.2, 145.3, 132.6, 132.3, 128.4, 128.1, 127.8, 126.6, 126.5, 121.8, 119.1, 114.9, 114.3, 68.9, 22.0, 10.5.

Synthesis of 4-(9,9-Dipropyl-9*H*-fluoren-2-yl)-2-(4-(9,9-dipropyl-9*H*-fluoren-2-yl) pyridin-2-yl)pyridine (3). Compound **3** was synthesized according to the same procedure of **2** except that used another intermediate, giving a white crystal of **3**. Yield: 42.9%. Mp: 278−280 °C; IR (KBr): 2939, 2856, 1589, 1455, 1286, 1253, 1187 cm^{-1}; ^1H NMR (400 MHz, $CDCl_3$): δ 8.80−8.68 (m, 4H), 7.77−7.65 (m, 8H), 7.63−7.58 (m, 2H), 7.36−7.23 (m, 6H), 2.03−1.91 (m, 8H), 0.70−0.51 (m, 20H); ^{13}C NMR (100 MHz, $CDCl_3$): δ 171.3, 151.8, 151.3, 149.6, 142.5, 140.4, 137.0, 127.7, 127.1, 126.4, 123.1, 122.0, 121.5, 120.3, 120.2, 119.5, 60.5, 55.7, 53.5, 42.9, 33.2, 21.2, 17.3, 14.6, 14.3.

Synthesis of cis-bis(Thiocyanato)(2,2′-bipyridyl-4,4′-dicarboxylato){4,4′-bis(9,9-dipropyl-9*H*-fluoren-2-yl)-2,2′-bipyridine}-ruthenium(II) (XS49). Compound XS49 was synthesized according to the same procedure of XS48, except that **3** was used instead of **2**. Yield: 44.3%. IR (KBr): 3417, 2955, 2105, 1959, 1612, 1465, 1363, 1020 cm^{-1}. ^1H NMR (DMSO-d_6, 300 MHz) δ: 9.42−8.62 (m, 8H), 8.54−7.82 (m, 12H), 7.68 (d, J = 8.7 Hz, 2H), 7.49 (dd, J = 8.7, 2.4 Hz, 2H), 7.37 (dd, J = 8.7, 2.4 Hz, 2H), 2.02 (m, 8H), 1.31 (m, 8H), 0.63 (t, J = 7.2 Hz, 12H); ^{13}C NMR (DMS-d_6, 300 MHz) δ: 164.9, 163.6, 157.6, 156.8, 156.3, 155.6, 150.3, 150.2, 149.7, 145.9, 145.1, 141.6, 141.2, 138.9, 138.6, 133.7, 133.6, 132.6, 132.2, 127.0, 126.1, 125.7, 122.2, 120.9, 119.7, 55.0, 41.5, 17.0, 14.3.

Optical and Electrochemical Measurements. The absorption spectra of the dyes either in solution or on the adsorbed TiO_2 film were measured by JASCO V-550 spectrophotometer. Fluorescence measurements were carried out with a HITACHI F-4500 fluorescence spectrophotometer. FT−IR spectra were obtained with a Bio-Rad FTS 135 FT−IR instrument.

Cyclic voltammetry measurements for dye-sensitized films were performed at room temperature on a computer controlled PARSTAT 2273 electrochemical workstation with dye-sensitized TiO_2 film on conducting glass as the working electrode, Pt-wires as the counter electrode, and an Ag/AgCl electrode as the reference electrode at a scan rate of 50 mV s^{-1}. Tetrabutylammonium perchlorate (TBAP, 0.1 mol/L) and MeCN were used as supporting electrolyte and solvent, respectively. The measurements were calibrated using ferrocene as standard. The redox potential of ferrocene internal reference is taken as 0.63 V vs NHE.[38] Electrochemical impedance spectroscopy (EIS) in the frequency range of 100 mHz to 100 kHz was performed with a PARSTAT 2273 potentiostat/galvanostat/FRA in the dark with the alternate current amplitude set at 10 mV.

Fabrication and Characterization of DSCs. The TiO_2 paste (particle size, 20 nm) consisting of 18 wt % TiO_2, 9 wt % ethyl cellulose, and 73 wt % terpineol was first prepared, which was printed on a conducting glass (Nippon Sheet Glass, Hyogo, Japan, fluorine-doped SnO_2 over layer, sheet resistance of 10 Ω/sq) using a screen printing technique. The film was dried in air at 120 °C for 30 min and calcined at 500 °C for 30 min under flowing oxygen before cooling to room temperature. The heated electrodes were impregnated with a 0.05 M titanium tetrachloride solution in a water-saturated desiccator at 70 °C for 30 min and fired again to give a ca. 12 μm thick mesoscopic TiO_2 film. The TiO_2 electrode was stained by immersing it into a dye solution containing 500 μM XS48/49 (DCM/ethanol (1:1)) for 12 h at room temperature. Then, the sensitized electrodes were rinsed with dry ethanol and dried by a dry air flow. Pt catalyst was deposited on the FTO glass by coating with a drop of H_2PtCl_6 solution (40 mM in ethanol) with the heat treatment at 395 °C for 15 min to give photoanode. The dye-covered TiO_2 electrode and Pt-counter electrode were assembled into a sandwich type cell by a 25 μm thick Surlyn (DuPont) hot-melt gasket and sealed up by heating. The electrolyte is composed of 1.0 M 1,3-dimethylimidazolium (DMII), 30 mM iodine (I_2), 1.0 M 4-tert-butylpyridine (TBP), and 0.1 M guanidinium thiocyanate (GNCS) in acetonitrile.

The photocurrent−voltage (J−V) characteristics of the solar cells were carried out using a Keithley 2400 digital source meter controlled by a computer and a standard AM 1.5 solar simulator-Oriel 91160−1000 (300W) SOLAR SIMULATOR 2 × 2 BEAM. The light intensity was calibrated by an Oriel reference solar cell. A metal mask with an aperture area of 0.16 cm^2 was covered on a testing cell during all measurements. The action spectra of monochromatic incident photon-to-current conversion efficiency (IPCE) for solar cell were performed using a commercial setup (QTest Station 2000 IPCE Measurement System, CROWNTECH, USA).

RESULTS AND DISCUSSION

We have synthesized the two ruthenium sensitizers XS48 and XS49 by the stepwise synthetic protocol illustrated in Scheme 1. There are two key starting compounds, 4,4,5,5-tetramethyl-2-(4-propoxyphenyl)-1,3,2-dioxaborolane and 2-(9,9-dipropyl-9*H*-fluoren-2-yl)-4,4,5,5-tetramethyl-1,3,2-dioxaborolane (see Supporting Information), for the synthesis of two ruthenium sensitizers. The Suzuki coupling reaction of 4,4′-dibromo-2,2′-bipyridyl with these two key compounds gave **2** and **3**, respectively. XS48 and XS49 were synthesized in an one-pot reaction from the sequential reaction of $[Ru(p\text{-cymene})Cl_2]_2$ with **2** and **3**, respectively, followed by the reaction of the resulting ruthenium complex with 4,4′-dicarboxyl-2,2′-bipyridine. The reaction of dichlororuthenium complexes (**6** and **7**) with an excess of ammonium thiocyanate afforded the ruthenium sensitizers XS48 and XS49. The two dyes were spectroscopically characterized, and all data are consistent with the formulated structure.

Photophysical and Electrochemical Properties. The absorption spectrum of XS48 and XS49 are measured in DMF solvent and compared with that of standard N3 absorption spectrum (Figure 2a). Table 1 summarizes the photophysical

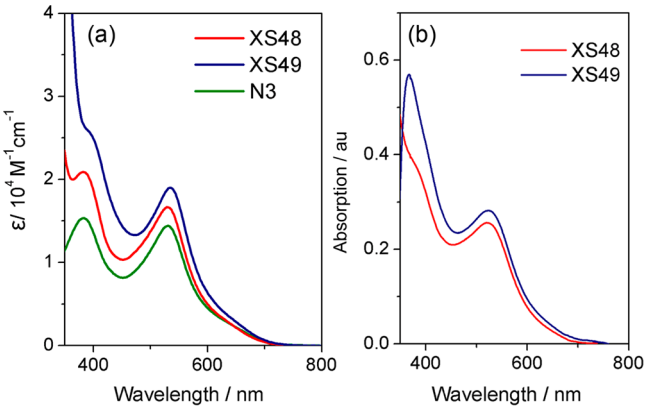

Figure 2. (a) Absorption spectra of dyes in DMF and (b) adsorbed on TiO_2 film (3 μm).

Table 1. Optical Properties and Electrochemical Properties of the Dyes

dye	λ_{max}/nm (ε/$M^{-1}cm^{-1}$)[a]	E_{0-0}/eV[b]	$E_{D/D+}$/V vs NHE[c]	$E_{D^*/D+}$/V vs NHE[d]
XS48	534 (16 500)	2.10	0.93	−1.17
XS49	531 (19 000)	2.09	0.91	−1.18
N3	530 (14 500)	2.13	0.96	−1.17

[a]The absorption spectra were measured in DMF solutions. [b]E_{0-0} values were estimated from the intersections of normalized absorption and emission spectra in DMF (Figure S1, Supporting Information), λ_{int}: E_{0-0} = 1240/λ_{int}. [c]The $E_{D/D+}$ (vs NHE) was measured in acetonitrile. [d]$E_{D^*/D+}$ was estimated from calculated $E_{D^*/D+} = E_{D/D+} - E_{0-0}$.

properties of all the as-synthesized dyes. Two absorption bands of XS48 and XS49 at 380 and 535 nm are the characteristic MLCT (metal-to-ligand charge transfer). The low energy MLCT band of both dyes is slightly red-shifted relative to that of N3. The molar extinction coefficient (ε) of the lower energy MLCT band for XS48 (ε = 16 500 M^{-1} cm^{-1}) and XS49 (ε = 19 000 M^{-1} cm^{-1}) are higher than that of N3 (ε = 14 500 M^{-1} cm^{-1}). This can be attributed to the introduction of the extended π-conjugation in combination with the butyloxy-substituted benzene ring and 9,9-dipropyl-9H-fluorene unit enhancing the local dipolar character of the ligand. Clearly, the light harvesting of the latter is superior to former in terms of the λ_{max} and ε. The absorption spectra of XS48 and XS49 on a TiO_2 film (3 μm) are broadened because of the interaction of the anchoring group with the surface titanium ion,[9b] ensuring a good light-harvesting efficiency (Figure 2b).

To obtain and understand the molecular orbital energy levels, cyclic voltammetry (CV) was carried out in a typical three-electrode electrochemical cell with TiO_2 film stained with sensitizer as the working electrode. As shown in Figure 3, the oxidation of XS48, XS49, and N3 are quasi-reversible. This phenomenon was also observed by other groups,[24,31,39] and a reasonable explanation is that the oxidation potential of the thiocyanate ligand is close to that of Ru(II).[39] The oxidation potentials ($E_{D/D+}$, corresponding to the HOMO level of dyes) of the XS48 and XS49 sensitizers adsorbed on TiO_2 films are 0.93 and 0.91 V vs NHE, respectively, which is assigned to the Ru(II)/Ru(III) couple, whereas the experimentally determined oxidation potential of N3 using the same experimental conditions gave 0.96 V vs NHE. The 0.03−0.05 V cathodic shift of the XS48 and XS49 oxidation potentials relative to that of N3 is attributed to the influence of the electron-donor nature of the substituents on the ancillary ligand in both sensitizers. Note that both the oxidation

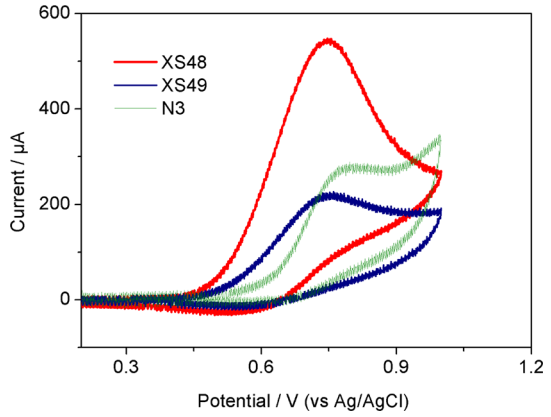

Figure 3. Cyclic voltammograms of the dye-loaded TiO_2 films for XS48, XS49, and N3.

potentials of XS48 and XS49 are more positive than that of the I^-/I_3^- redox couples (0.4 V vs NHE[40]). Recently, studies suggest that 0.5−0.6 eV driving force is needed for regeneration of Ru complex sensitizers in iodide/triiodide electrolyte.[41] Therefore, the driving forces are sufficient for both dyes' regeneration. On the other hand, the LUMO levels for XS48 and XS49 (−1.17 and −1.18 V, respectively) are more negative than the conduction band of TiO_2 (−0.5 V vs NHE[42]), which provided sufficient driving forces for electron injection.

Computational Analysis. To further confirm the electron distribution of the HOMO and LUMO, we optimized the geometry of the XS48 and XS49 sensitizer using a mixed basis set: Lanl2dz for Ru atom, B3LYP for other atoms. As displayed in Figure 4, the HOMO and HOMO−1 for both dyes have a

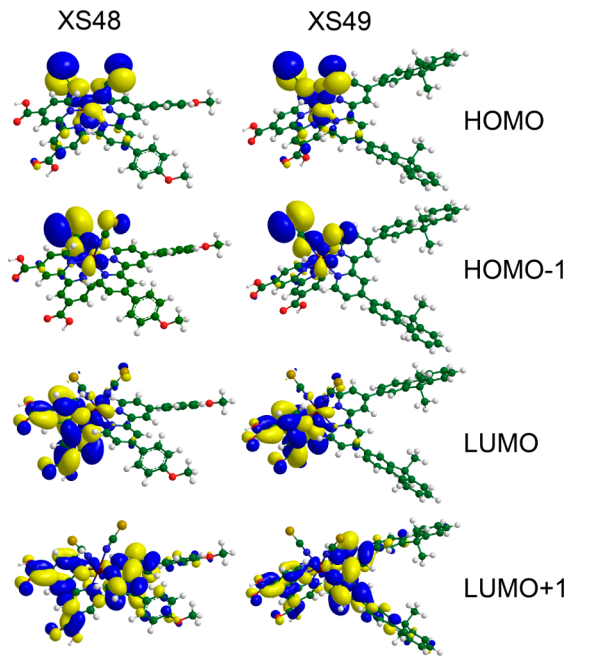

Figure 4. Isodensity surface plots of the HOMO, HOMO−1, LUMO, and LUMO+1 of XS48 and XS49.

ruthenium excited state (t_{2g}) character in addition to a sizable population from the thiocyanate with a significant contribution on the far-end sulfur atom. The LUMOs of both dyes are predominately delocalized over the dcbpy (dcbpy = 4,4′-dicarboxy-2,2′-bipyridyl)

dx.doi.org/10.1021/am302318z | ACS Appl. Mater. Interfaces 2013, 5, 144−153

ligand and ruthenium center. Unlike the LUMO, the LUMO+1 of both dyes are a combination of the π-bonding orbital of the dcbpy and the ruthenium center, appreciably mixed with the bpy (bpy = 2,2′-bipyridyl) of the ancillary ligand. The HOMO−LUMO excitation transfers the electrons from the NCS ligands to the anchoring ligand (dcbpy) by photoexcitation and, therefore, results in an efficient electron injection.

Photovoltaic Performance of DSCs. Photovoltaic tests were conducted to evaluate the potential of the XS48 and XS49 dyes in DSCs. The $J-V$ curves for the DSCs based on XS48 and XS49 are presented and compared with that of the N3 dye in Figure 5. The detailed photovoltaic parameters are summarized

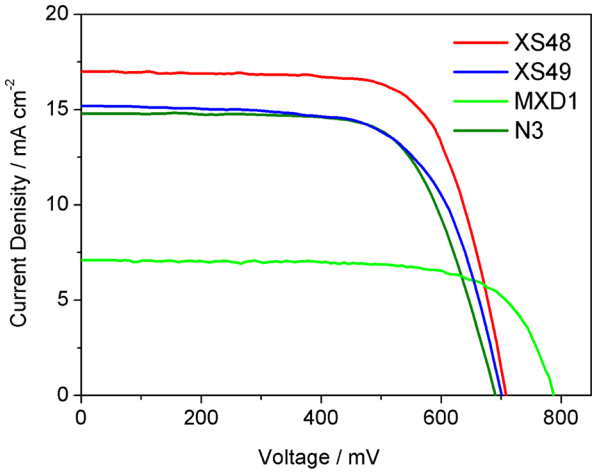

Figure 5. $J-V$ curves of DSCs based on XS48, XS49, MXD1, and N3.

in Table 2. The XS48 and XS49 sensitized cell gave short circuit photocurrent densities (J_{SC}) of 17.0 and 15.2 mA cm^{-2}, open

Table 2. Photovoltaic Performance of DSCs

dye	J_{SC} (mA cm^{-2})	V_{OC} (mV)	FF	PCE (%)
XS48	17.0	708	0.69	8.30
XS48→MXD1	16.8	726	0.68	8.29
XS48+MXD1	16.0	685	0.70	7.67
XS48+CDCA	15.7	688	0.69	7.45
XS49	15.2	700	0.67	7.12
XS49→MXD1	16.1	735	0.69	8.16
XS49+MXD1	15.7	690	0.68	7.37
XS49+CDCA	15.4	710	0.68	7.43
MXD1	7.1	780	0.69	3.82
N3	14.8	690	0.69	7.04

circuit voltages (V_{OC}) of 708 and 700 mV, and fill factors (FF) of 0.69 and 0.67, corresponding to overall power conversion efficiencies (PCE) of 8.30 and 7.12%, respectively. Both the dyes exhibited superior performance related to the N3, which sensitized-cell gave a J_{SC} of 14.8 mA cm^{-2}, a V_{OC} of 690 mV, and a FF of 0.69, corresponding to PCE of 7.04% under the same condition. The PCE enhancement of XS48 and XS49 relative to N3 can be ascribed to the improved J_{SC} due to expansion of the π-conjugated system of them. Compared to the butyloxy-substituted benzene ring counterpart (XS48), a J_{SC} attenuation of 1.8 mA cm^{-2} (15.2 vs 17.0 mA cm^{-2}) can be noted upon the substitution with the 9,9-dipropyl-9H-fluorene group (XS49).

To clarify the above results, we have measured the amounts adsorbed on the TiO_2 film by comparing the absorbance change of a dye solution (500 μM) before and after dye uptake with a titania film (see Table 3). The surface coverage (Γ) of XS49

Table 3. Adsorbed Amounts of Dyes and MXD1

dye	dye adsorbed amount (mol/cm^2)	MXD1 adsorbed amount (mol/cm^2)	total amount (mol/cm^2)
XS48	3.39×10^{-7}		
XS48→MXD1	3.20×10^{-7}	0.49×10^{-7}	3.69×10^{-7}
XS48+MXD1	1.78×10^{-7}	1.21×10^{-7}	2.99×10^{-7}
XS48+CDCA	2.93×10^{-7}		
XS49	2.72×10^{-7}		
XS49→MXD1	2.59×10^{-7}	0.55×10^{-7}	3.14×10^{-7}
XS49+MXD1	1.51×10^{-7}	1.16×10^{-7}	2.67×10^{-7}
XS49+CDCA	2.52×10^{-7}		
MXD1		1.34×10^{-7}	

(2.72×10^{-7} mmol cm^{-2}) is lower than that of XS48 (3.39×10^{-7} mmol cm^{-2}), which can be attributed to the presence of more bulky 9,9-dipropyl-9*H*-fluorene groups. Thus, more intense light absorption could be expected, which attributed to higher IPCE of XS48 related to that of XS49 (Figure 6a,b).

Besides the impact on surface coverage, the ancillary ligands also have an influence on the surface blocking of dyes on the TiO_2. It is found that the electron recombination occurs more significantly in the photoelectrode adsorbing the ruthenium dyes with more bulky ancillary ligands, owing to the relatively large TiO_2 surface areas unoccupied by dye molecules, which adversely influences the V_{OC}.[22,30,31] Garćıa-Iglesias et al. reported two novel heteroleptic ruthenium sensitizers,[30] TT204 and TT205, containing bulky substituents at the 4,4′-positions of the ancillary 2,2′-bipyridine ligand. They observed that both dyes on thick 12 + 5 μm films sensitized in the presence of chenodeoxycholic acid (CDCA) generated higher J_{SC} of 18.2 mA cm^{-2} (TT204) and 18.7 mA cm^{-2} (TT205) than the published value of 17.9 mA cm^{-2} for the C101 dye. However, V_{OC} decreased to a much greater extent (780, 680, and 720 mV for C101, TT204, and TT205 respectively). They attributed this to the disordered dye packing on the TiO_2 surface when dye contains large bulky groups.

To examine the influence arising from the bulky ancillary ligands and to alleviate the electron recombination mentioned above, we developed a truxene-based triarylamine dye (MXD1, see Figure 7) to use as a coadsorbent for XS48- and XS49-sensitized DSCs. In our previous study,[43−46] we found that the hexapropyl-truxene group on the dyes retarded the rate of interfacial back electron transfer from the conduction band of the nanocrystalline titanium dioxide film to the I_3^- ions, which enabled attainment of high photovoltage approaching 800 mV.

To realize coadsorption, a traditional approach is simultaneous adsorption of the dyes and coadsorbent.[47−50] In other words, the TiO_2 film adsorbed the coadsorbent and dye simultaneously (Scheme 2a). The advantage of this approach can suppress dye aggregation and reduction of charge recombination. Nevertheless, coadsorbent may induce competitive adsorption. Recently, sequential adsorption, as an impressive cosensitization methodology, was introduced by several groups.[51−53] By this way, the related electrodes were obtained by dipping TiO_2 film into a first dye solution, followed by immersing it in a another dye solution (Scheme 2a). The key features of this approach are that the sequence of dye adsorption and the stained time of a different kind of dye can be controlled and a subtle tuning can thus be realized. However, the effect of sequential adsorption for coadsorption has not yet been addressed. It is interesting to

dx.doi.org/10.1021/am302318z | ACS Appl. Mater. Interfaces 2013, 5, 144−153

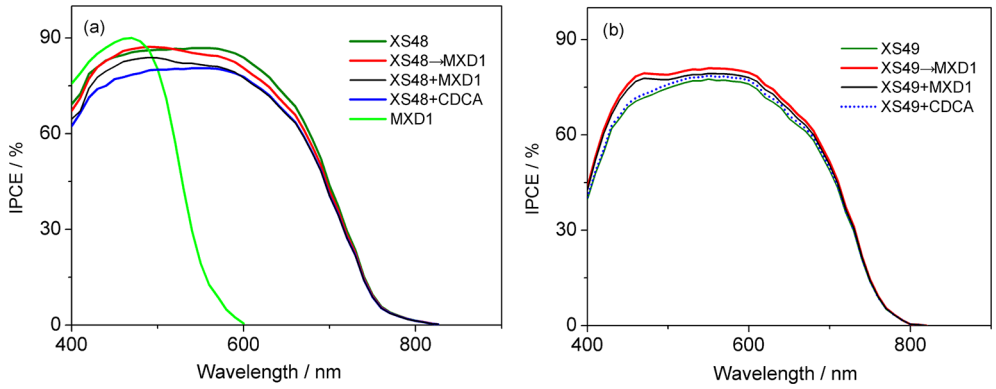

Figure 6. IPCE spectra of DSCs based on XS48/49, XS48/49→MXD1, XS48/49+MXD1, XS48/49+CDCA, and MXD1.

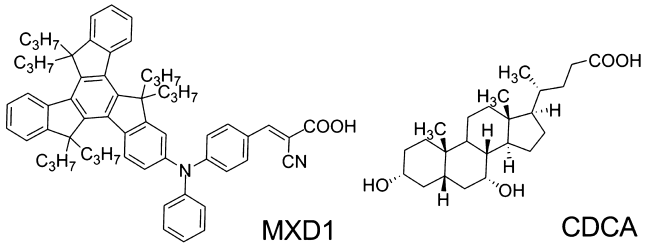

Figure 7. Molecular structures of MXD1 and CDCA.

Scheme 2. (a) Typical Process of the Simultaneous Adsorption and the Sequential Adsorption; (b) the Front and Back View of TiO_2 Film Stained in XS49 for 12 h

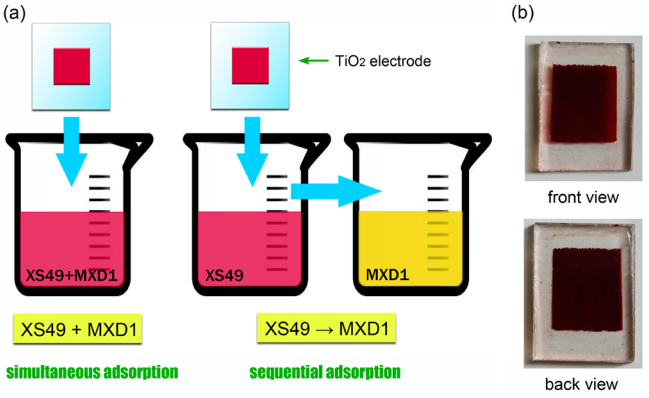

investigate the influence of the coadsorption pattern on the performance of XS48- and XS49-sensitized DSCs. For the first approach, the TiO_2 electrode was stained in a mixed solvent of DCM and ethanol (1:1 v/v) containing 500 μM XS48/XS49 and 120 μM MXD1 for 12 h, namely, XS48/49+MXD1. For the second approach, a TiO_2 electrode was dipped in XS48/49 solution (500 μM in DCM/ethanol (1:1)) for 12 h, rinsed with ethanol, and dipped in MXD1 solution (500 μM in DCM/ethanol (1:1)) for another 12 h, namely, XS48/49→MXD1.

Besides the coadsorption approach, the thickness of TiO_2 film is another factor that needs to be considered in our experiments. Ko and co-workers proposed that the penetration of ruthenium dyes with bulky structure into the thick TiO_2 film could be restrained by its extended molecular size.[53] For the second approach, it is therefore possible that the enlarged structure of the ruthenium complex molecules is allowed to position them on the upper side of a nanoporous TiO_2, and the small coadsorbents will mainly be positioned on the inner side of the TiO_2 film. In contrast, for the first approach, the small coadsorbent is distributed averagely on the entire TiO_2 film. Bare TiO_2 surface areas arising from bulky ancillary ligands exist not only in the inner side of the TiO_2 film but also in the upper side of TiO_2 electrodes. To avoid the difference mentioned above, 12 μm TiO_2 electrodes were employed in our experiments. We found that the back side of TiO_2 electrode was fully stained after a 12 h dipping for both dyes (e.g., XS49-sensitized film, Scheme 2b). This observation suggests that dyes XS48 and XS49 have penetrated the TiO_2 film, and MXD1 are just adsorbed on bare TiO_2 surface areas arising from bulky ancillary ligands.

As shown in Figure 8a,b, XS48/49→MXD1 is superior to XS48/49+MXD1 in terms of not only J_{SC} but also V_{OC}. Particularly, compared with XS48/49+MXD1, XS48/49→MXD1 successfully realized a significant increase in V_{OC} about 40 mV. Note that the voltage advantage of XS48/49→MXD1 over XS48/49+MXD1 is maintained as the concentration of MXD1 decreases or increases (Table S1 in the Supporting Information). In addition, we make a comparison between the XS48/49 (708 and 700 mV, respectively) and XS48/49→MXD1 (726 and 735 mV, respectively). Higher V_{OC} value of the XS48/49→MXD1 suggests evidently that there are some TiO_2 surface areas unoccupied by XS48/49, especially regarding XS49, which is consistent with the surface coverage measurements (Table 3). As a result, more compact sensitizers could be established on the TiO_2 surface by sequential adsorption of XS48/49 and MXD1.

It is well-known that the presence of CDCA in the dye solution during the sensitization can form a shielding of the surface against electron recombination. In parallel with the studies on XS48/49+MXD1 and XS48/49→MXD1, CDCA was introduced for evaluating the role of the MXD1 as coadsorbent. That is, the TiO_2 electrode was stained by immersing into a mixed solvent of DCM and ethanol (1:1 v/v) containing 500 μM XS48/XS49 and 1.0 *m*M CDCA for 12 h, namely, XS48/49+CDCA. As seen from Table 2, for the XS48 and XS49, the (dye→MXD1)-to-(dye+CDCA) approach alteration has caused V_{OC} reductions of 38 and 25 mV, respectively, accounting for the observed PCE decreasing. As the concentration of CDCA is increased, the corresponding V_{OC} values improved slightly, while the J_{SC} values decreased (e.g., in the case of XS49+CDCA, when CDCA = 2.0 *m*M, V_{OC} = 716 mV, J_{SC} = 15.1, FF = 0.69, PCE = 7.46%). This result demonstrates that this new class of truxene-based organic coadsorbent (MXD1) can be used as an alternative coadsorbent to CDCA in ruthenium dye-sensitized DSCs, authenticating our motif to attenuate charge recombination by coadsorption of ruthenium dyes with bulky structure and organic coadsorbent.

dx.doi.org/10.1021/am302318z | ACS Appl. Mater. Interfaces 2013, 5, 144−153

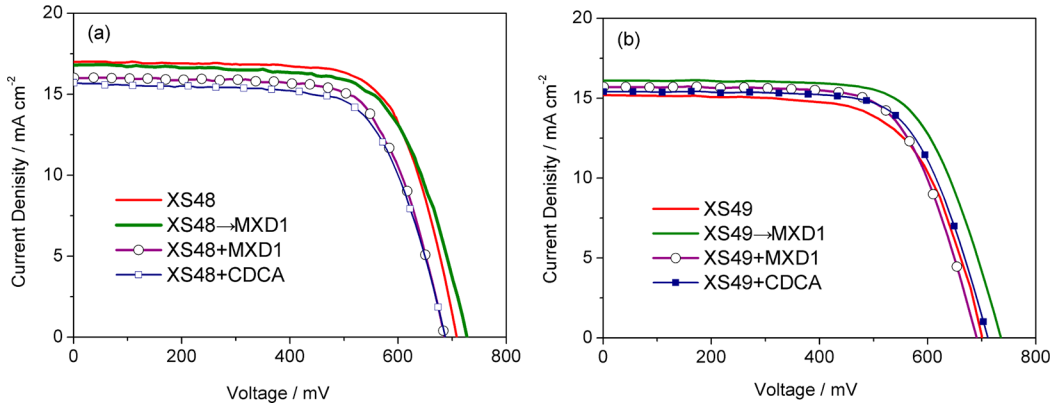

Figure 8. $J-V$ curves of DSCs under AM 1.5G simulated solar light (100 mW cm $^{-2}$).

Unlike the trend observed in variation of V_{OC}, the addition of coadsorbent resulted in a contrary influence on J_{SC} for XS48- and XS49-based DSCs. That is, the XS48 to XS48→MXD1/XS48+MXD1/XS48+CDCA alteration has caused a J_{SC} attenuation of 0.2−1.3 mA cm^{-2}, contrasting a 0.2−0.9 mA cm^{-2} enhancement observed for XS49 to XS49→MXD1/XS49+MXD1/XS49+CDCA alteration. As a result, the photovoltaic performance of XS48 containing butyloxy-substituted benzene ring was independent of the coadsorbents MXD1 and CDCA. In contrast, the coadsorbents are beneficial for XS49. XS49→MXD1, XS49+MXD1, and XS49+CDCA bring forth a 14.6%, 3.5%, and 4.3% enhancement of PCE relative to that of XS49, respectively.

The J_{SC} enhancement of XS49→MXD1 related to XS49 is mainly attributed to the retardation of interfacial charge recombination (see next section) and a large increase of the total amount of dye adsorption. As listed in Table 3, the total amount of dye adsorption was increased from 2.72×10^{-7} mol/cm^2 to 3.14×10^{-7} mol/cm^2 by coadsorption with MXD1. As presented in Figure 6b, the IPCE values of XS49→MXD1-based DSCs increased, especially in the range of 400−490 nm. Clearly, MXD1 contributed to the stronger absorption around 465 nm in the IPCE spectrum. MXD1 has dual functioned effects in the case of XS49→MXD1. It not only acts as insulating molecular layer which effectively shields the back electron transfer from the TiO_2 to I_3^- ions but also has the light harvesting effect in the short wavelength region. In contrast, the mechanism of J_{SC} enhancement inducing by XS49+CDCA is different from that by XS49→MXD1. A combined effect of diminishing the aggregation formation between the dye molecules onto TiO_2 and a slow charge recombination at the titania/electrolyte interface (see next section) are thought to be responsible for this observation.[54,55]

As shown in Table 3, simultaneous adsorption of the ruthenium dyes and MXD1/CDCA has caused a reduced total adsorption amount of ruthenium dyes due to competitive adsorption. It is valuable to note that the more serious drops in total dye adsorption were observed in the case of XS48+MXD1 (decreased by about 11.7%) and XS48+CDCA (decreased by about 13.5%) when compared to those of XS49+MXD1 (decreased by about 1.8%) and XS49+CDCA (decreased by about 7.3%), respectively. The J_{SC} attenuation of XS48+MXD1 and XS48+CDCA related to XS48 can partially be a result of the significant reduction of a total adsorption amount of dyes on the TiO_2 surface.

Electrochemical Impedance Spectroscopy. As discussed above, the V_{OC} variation arising from the coadsorbent is intriguing. To scrutinize the origin of the coadsorbent on the variation of V_{OC}, measurements of the electrochemical impedance spectroscopy (EIS) were performed. The chemical capacitance (C_μ) and interfacial charge transfer resistance (R_{CT}) were obtained by fitting the experimental data of all of the samples with an equivalent circuit reported (Figure S2 in the Supporting Information).[56]

As commonly understood, the V_{OC} of a DSC intrinsically represents the difference between Fermi-level of TiO_2 ($E_{F,n}$) and Fermi-level of a redox electrolyte ($E_{F,redox}$), i.e., $V_{OC} = E_{F,redox} - E_{F,n}$.[57] On the other hand, the $E_{F,n}$ of TiO_2 can be expressed as

$$E_{F,n} = E_{CB} + k_B T \ln\left(\frac{n_c}{N_c}\right) \quad (1)$$

where k_B is the Boltzmann constant, T is the temperature (293 K in this work), n_c is the free electron density, and N_c is the density of accessible states in the conduction band.[58] Considering that $E_{F,redox}$ would not change strongly in DSCs with a fixed redox electrolyte, V_{OC} is intimately correlated to the E_{CB} and n_c.

To figure out the influence of coadsorbent on E_{CB}, we first derived the chemical capacitance of a mesoporous titania film through measuring the EIS of our cells, which can be expressed as an exponential function of potential bias. This exponential rise with the increase of forward bias is a behavior of typical C_μ that is described by eq 2[59,60]

$$C_\mu = \frac{e^2}{K_B T} \exp\left[\frac{\alpha}{K_B T}(E_{F,redox} + eV_a - E_{CB})\right] \quad (2)$$

where e is elementary charge and α is a constant related to the distribution of localized states below the conduction band. Considering that $E_{F,redox}$ would not change strongly in DSCs with a fixed redox electrolyte, the C_μ is governed by the applied potential (V_a) and E_{CB}.

As indicated in Figure 9a, at a given value of V_a, the C_μ for these dyes are in the order of XS48+MXD1 > XS48+CDCA > XS48 ≈ XS48→MXD1, indicating a sequential positive shift of the E_{CB}.[44] Generally, positive shift of E_{CB} leads to a V_{OC} loss for DSCs. Therefore, the sequence of conduction band movement is consistent with the sequence of V_{OC} values in the devices. The same trend in C_μ was also found for cells prepared from XS49, XS48→MXD1, XS49+MXD1, and XS48+CDCA (Figure 9b). These results suggest that the movement E_{CB} for the above cells is partially responsible for the variation of V_{OC}.

The charge recombination resistance at the TiO_2/electrolyte interface was further modeled from impedance spectroscopies as a function of potential bias. The R_{CT} is related to the charge recombination rate, such that a smaller R_{CT} means the larger charge recombination rate. As presented in Figure 9c, the fitted

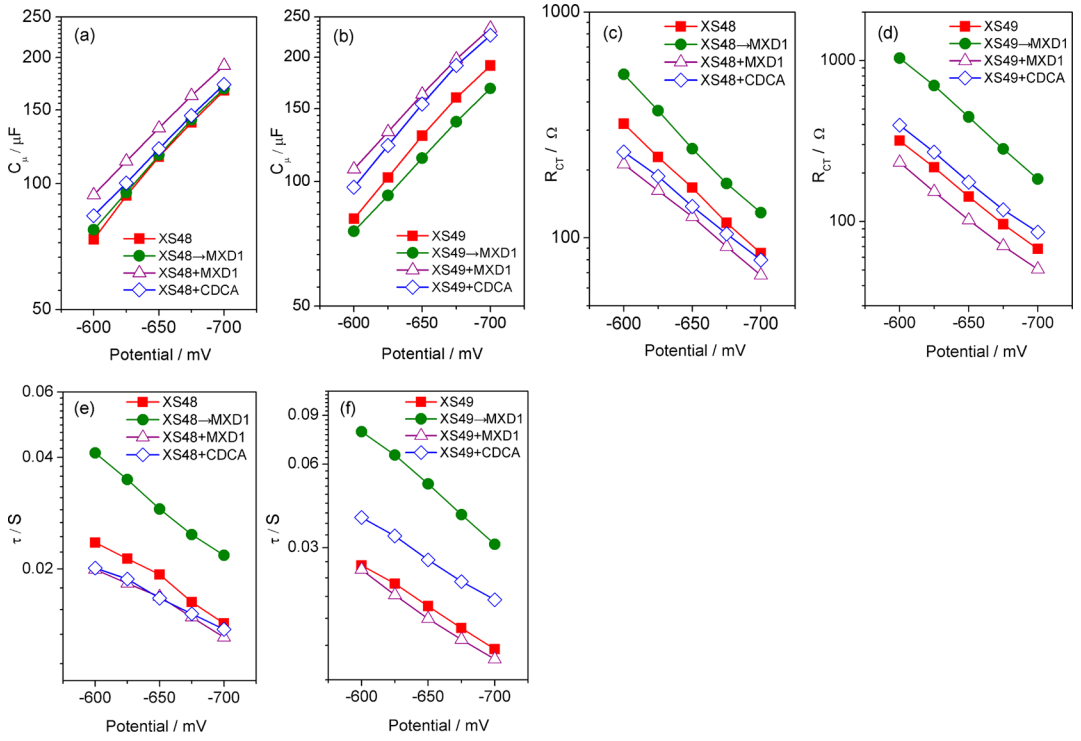

Figure 9. Plots of C_μ (a,b), R_{CT} (c,d), and τ (e,f) versus potential bias of DSCs based on XS48 and XS49.

R_{CT} increases in the order of XS48+MXD1 < XS48+CDCA < XS48 < XS48→MXD1, indicating a same order of decreased charge recombination rate. On the other hand, the alteration of coadsorbents has caused the fitted R_{CT} increases in the order of XS49+MXD1 < XS49 < XS49+CDCA < XS49→MXD1.

By fitting the EIS curves, another important parameter for DSCs, electron lifetime (τ), could be extracted from the C_μ and R_{CT} using $\tau = C_\mu R_{CT}$.[61,62] In contrast to the XS48/49 sensitized cells, the XS48/49→MXD1 congeners exhibit evidently enhanced electron lifetime at a given potential bias, i.e., a retardation of charge recombination at the titania/electrolyte interface. Moreover, it can be found from Figure 9e,f that the electron lifetimes of DSCs based on XS48/49+MXD1 and XS48/49+CDCA are much shorter than that of XS48/49→MXD1 counterparts. These observations suggest that sequential adsorption of MXD1 onto the TiO_2 surface had resulted in the formation of a compacted dye layer that could effectively suppress the recombination of electrons in the TiO_2 film with I_3^- ions. The successful exploitation of coadsorbent MXD1 provided us with a new direction for developing novel ruthenium dyes with bulky structure that can increase not only the V_{OC} but also the IPCE in the wavelength region to further enhance solar cell efficiency.

We further examined the effect of triiodide concentration on the charge recombination. In Figure 10, the V_{OC} as a function of I_2 concentration (30, 100, and 300 mM) is plotted for XS48/49, XS48/49→MXD1, XS48/49+MXD1, XS48/49+CDCA solar cells. The discrepancy in the V_{OC} is thus dependent on how the different coadsorbents affect the recombination processes. As expected, the V_{OC} clearly decrease with increased I_2 concentration. This V_{OC} reduction can be attributed to the increased concentration of acceptor species in the electrolyte, increasing the probability of electron recombination. As summarized in Table 4, the V_{OC} difference for the different cells at high I_2 concentration is smaller than those of cells at low I_2 concentration. For example, XS49→MXD1 confers a 25 mV augmentation of cell photovoltage

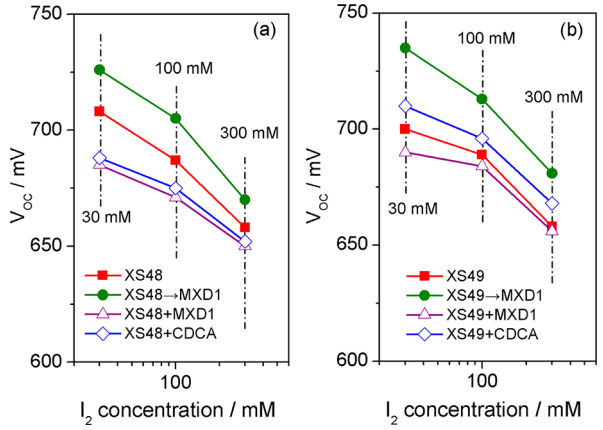

Figure 10. V_{OC} of DSCs based on XS48 (a) and XS49 (b) as a function of I_2 concentration.

related to XS49+MXD1 when the I_2 concentration increased to 300 mM, contrasting a 45 mV enhancement at low I_2 concentration (30 mM). This observation indicates that the blocking effect of coadsorbents is weak as the I_2 concentration increases. In spite of that, it is noteworthy that the advantage in voltage of XS48/49→MXD1 is maintained at high I_2 concentration, up to 300 mM, proving the superiority of the sequential adsorption of MXD1 onto the TiO_2 surface.

The superiority of XS48/49→MXD1 regarding reduction of charge recombination can be understood from the structure of the molecule: as illustrated in Figure 11, the chemical structure of MXD1 has a bulkier structure than CDCA, especially regarding the top view of the molecule. MXD1 with considerably large "protected" area (approximated 119 Å^2) can readily block the acceptor species in the electrolyte approaching the TiO_2 surface, thereby suppressing electron recombination. However, we should bear in mind that organic dyes with bulky structure are liable to

dx.doi.org/10.1021/am302318z | ACS Appl. Mater. Interfaces 2013, 5, 144−153

Table 4. V_{OC} Variation of Cells with Different I_2 Concentration

dye	V_{OC} (mV)[a]	V_{OC} (mV)[b]	V_{OC} (mV)[c]
XS48	708	687	658
XS48→MXD1	726	705	670
XS48+MXD1	685	671	650
XS48+CDCA	688	675	652
XS49	700	689	658
XS49→MXD1	735	713	681
XS49+MXD1	690	684	656
XS49+CDCA	710	696	668

[a]30 mM I_2. [b]100 mM I_2. [c]300 mM I_2.

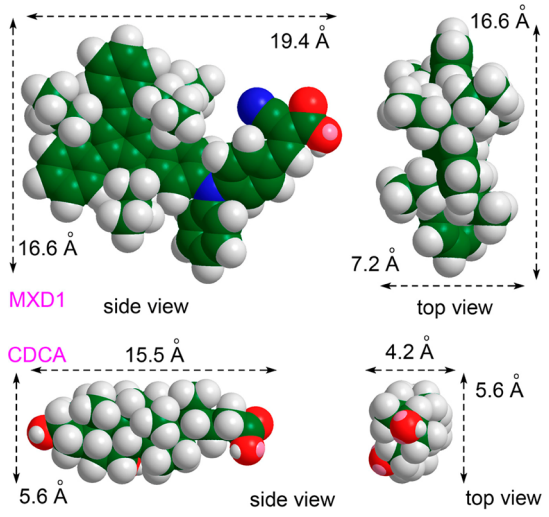

Figure 11. Molecular structures of MXD1 and CDCA derived from density functional theory (DFT) calculations (b3lyp).

experience competitive adsorption among dyes, which have an adverse effect on the photocurrent. Actually, a drop of ruthenium dye adsorption evokes not only a reduction of light harvesting but also an acceleration of interfacial charge recombination of the titania electrons with I_3^- ions, leading to an attenuated V_{OC}. For example, the efficiency attenuation for cells based on XS48+MXD1 and XS48+CDCA with respect to those of XS48 is most likely caused by the significantly reduced XS48 adsorption on the TiO_2 surface. Therefore, the key issue is to make the most of the advantage of MXD1 (i.e., good blocking effect) but avoid their competitive adsorption. A unique advantage of XS48/49→MXD1 is that higher V_{OC} can be realized without sacrificing the J_{SC}.

CONCLUSIONS

Two ruthenium complexes, XS48 and XS49, were synthesized, and their properties in solution and in DSC devices were investigated. The extended ancillary ligand gives rise to a slight red-shift of the lowest MLCT band as well as a relatively higher molar extinction coefficient with respect to N3. In addition, the DSCs based on XS48 and XS49 achieve better performance than those of N3-sensitized solar cell under the same cell fabrication, highlighting the strategy of incorporation of electron-rich unit in the ancillary ligands for improving the performance of the ruthenium dyes. On the other hand, we have developed MXD1 as a coadsorbent for XS48- and XS49-sensitized DSCs to examine the influence of the bulky ancillary ligand and alleviate the electron recombination. The XS48/49→MXD1 approach has displayed a significantly improved photovoltage, proving the superiority of employing sequential adsorption relative to simultaneous adsorption when bulky MXD1 was introduced. The photovoltaic performance of XS48-sensitized DSC was independent of the coadsorbent either MXD1 or CDCA, indicating that the butyloxy-substituted benzene ring induces a good dye packing on the TiO_2 surface. In contrast, when dye XS49 contains a large bulky ancillary ligand, coadsorbents are indispensable for achieving high efficiency. Evidently, MXD1 not only acts as an insulating molecular layer which effectively shields the back electron transfer from the TiO_2 to I_3^- ions but also has the light harvesting effect in the short wavelength region. These results emphasize the importance of the approach for selecting coadsorbent and will facilitate further improvement in the performance of the ruthenium complexes with bulky ancillary ligand.

ASSOCIATED CONTENT

Supporting Information

Synthesis and characterization of the 4,4,5,5-tetramethyl-2-(4-propoxyphenyl)-1,3,2-dioxaborolane and 2-(9,9-dipropyl-9*H*-fluoren-2-yl)-4,4,5,5-tetramethyl-1,3,2-dioxaborolane; Figures S1–S3 and Table S1. This material is available free of charge via the Internet at http://pubs.acs.org.

AUTHOR INFORMATION

Corresponding Author

*E-mail: liangmao717@126.com (M.L.); xuesong@ustc.edu.cn (S.X.). Tel.: +86 22 60214250. Fax: +86 22 60214252.

Notes

The authors declare no competing financial interest.

ACKNOWLEDGMENTS

We are grateful to the National Natural Science Foundation of China (21003096, 21072152) for financial support.

REFERENCES

(1) O'Regan, B.; Grätzel, M. *Nature* **1991**, *353*, 737–740.
(2) Nazeeruddin, M. K.; Kay, A.; Rodicio, I.; Humphry-Baker, R.; Mueller, E.; Liska, P.; Vlachopoulos, N.; Grätzel, M. *J. Am. Chem. Soc.* **1993**, *115*, 6382–6390.
(3) Nazeeruddin, M. K.; Zakeeruddin, S. M.; Humphry-Baker, R.; Jirousek, M.; Liska, P.; Vlachopoulos, N.; Shklover, V.; Fischer, C.-H.; Grätzel, M. *Inorg. Chem.* **1999**, *38*, 6298–6305.
(4) Nazeeruddin, M. K.; Pechy, P.; Renouard, T.; Zakeeruddin, S. M.; Humphry-Baker, R.; Comte, P.; Liska, P.; Cevey, L.; Costa, E.; Shklover, V.; Spiccia, L.; Deacon, G. B.; Bignozzi, C. A.; Grätzel, M. *J. Am. Chem. Soc.* **2001**, *123*, 1613–1624.
(5) Cao, M.; Bai, Y.; Cheng, Y.; Liu, S.; Shi, D.; Gao, F.; Wang, P. *J. Phys. Chem. C* **2009**, *113*, 6290–6297.
(6) Gao, F.; Wang, Y.; Shi, D.; Zhang, J.; Wang, M. K.; Jing, X. Y.; Humphry-Baker, R.; Wang, P.; Zakeeruddin, S. M.; Grätzel, M. *J. Am. Chem. Soc.* **2008**, *130*, 10720–10728.
(7) Bomben, P. G.; Robson, C. D.; Sedach, P. A.; Berlinguette, C. P. *Inorg. Chem.* **2009**, *48*, 9631–9643.
(8) Bomben, P. G.; Gordon, J. T.; Schott, E.; Berlinguette, C. P. *Angew. Chem., Int. Ed.* **2011**, *50*, 10682–10685.
(9) Li, G. C.; Bomben, P. L. G.; Robson, K. C. D.; Gorelsky, S. I.; Berlinguette, C. P.; Shatruk, M. *Chem. Commun.* **2012**, *48*, 8790–8792.
(10) Wu, K.-L.; Li, C.-H.; Chi, Y.; Clifford, J. N.; Cabau, L.; Palomares, E.; Cheng, Y.-M.; Pan, H.-A.; Chou, P.-T. *J. Am. Chem. Soc.* **2012**, *134*, 7488–7496.
(11) Wang, P.; Klein, C.; Humphry-Baker, R.; Zakeeruddin, S. M.; Grätzel, M. *J. Am. Chem. Soc.* **2005**, *127*, 808–809.
(12) Kuang, D. B.; Klein, C.; Ito, S.; Moser, J. E.; Humphry-Baker, R.; Evans, N.; Duriaux, F.; Grätzel, C.; Zakeeruddin, S. M.; Grätzel, M. *Adv. Mater.* **2007**, *19*, 1133–1137.

(13) Chandrasekharam, M.; Suresh, T.; Singh, S. P.; Priyanka, B.; Bhanuprakash, K.; Islam, A.; Han, L.; Kantam, M. L. *Dalton Trans.* **2012**, *41*, 8770−8772.
(14) Kuang, D.; Klein, C.; Ito, S.; Moser, J.-E.; Humphry-Baker, R.; Zakeeruddin, S. M.; Grätzel, M. *Adv. Funct. Mater.* **2007**, *17*, 154−160.
(15) Kim, C.; Choi, H.; Kim, S.; Baik, C.; Song, K.; Kang, M.-S.; Kang, S. O.; Humphry-Baker, J.; Ko, R.; Grätzel, M.; Nazeeruddin, M. K. *Inorg. Chem.* **2008**, *47*, 2267−2273.
(16) Sun, Y.; Onicha, A. C.; Myahkostupov, M.; Castellano, F. N. *ACS Appl. Mater. Interfaces* **2010**, *2*, 2039−2045.
(17) Matar, F.; Ghaddar, T. H.; Walley, K.; DosSantos, T.; Durrantb, J. R.; O'Regan, B. *J. Mater. Chem.* **2008**, *18*, 4246−4253.
(18) Kisserwan, H.; Kamar, A.; Shoker, T.; Ghaddar, T. H. *Dalton Trans.* **2012**, *41*, 10643−10651.
(19) Chen, C. Y.; Wu, S. J.; Wu, C. G.; Chen, J. G.; Ho, K. C. *Angew. Chem., Int. Ed.* **2006**, *45*, 5822−5825.
(20) Chen, C.-Y.; Chen, J.-G.; Wu, S.-J.; Li, J.-Y.; Wu, C.-G.; Ho, K.-C. *Angew. Chem., Int. Ed.* **2008**, *47*, 7342−7345.
(21) Yin, J.-F.; Chen, J.-G.; Lu, Z.-Z.; Ho, K.-C.; Lin, H.-C.; Lu, K.-L. *Chem. Mater.* **2010**, *22*, 4392−4399.
(22) Kim, J.-J.; Choi, H.; Kim, C.; Kang, M.-S.; Kang, H. S.; Ko, J. *Chem. Mater.* **2009**, *21*, 5719−5726.
(23) Kim, J.-J.; Lim, K.; Choi, H.; Fan, S. Q.; Kang, M.-S.; Gao, G. H.; Kang, H. S.; Ko, J. *Inorg. Chem.* **2010**, *49*, 8351−8357.
(24) Kim, J.-J.; Choi, H.; Paek, S.; Kim, C.; Lim, K.; Ju, M.-J.; Kang, H. S.; Kang, M.-S.; Ko, J. *Inorg. Chem.* **2011**, *50*, 11340−11347.
(25) Yu, Q. J.; Wang, Y. H.; Yi, Z. H.; Zu, N. N.; Zhang, J.; Zhang, M.; Wang, P. *ACS Nano* **2010**, *26*, 6032−6038.
(26) Wang, P.; Zakeeruddin, S. M.; Moser, J.-E.; Humphry-Baker, R.; Comte, P.; Aranyos, V.; Hagfeldt, A.; Nazeeruddin, M. K.; Grätzel, M. *Adv. Mater.* **2004**, *16*, 1806−1811.
(27) Abbotto, A.; Barolo, C.; Bellotto, L.; Angelis, F. D.; Grätzel, M.; Manfredi, N.; Marinzi, C.; Fantacci, S.; Yumd, J.-H.; Nazeeruddin, M. K. *Chem. Commun.* **2008**, 5318−5320.
(28) Gao, F.; Wang, Y.; Zhang, J.; Shi, D.; Wang, M.; Humphry-Baker, R.; Wang, P.; Zakeeruddin, S. M.; Grätzel, M. *Chem. Commun.* **2008**, 2635−2637.
(29) Chen, C. Y.; Wang, M. K.; Li, J. Y.; Pootrakulchote, N.; Alibabaei, L.; Ngoc-le, C. H.; Decoppet, J. D.; Tsai, J. H.; Gratzel, C.; Wu, C. G.; Zakeeruddin, S. M.; Grätzel, M. *ACS Nano* **2009**, *3*, 3103−3109.
(30) García-Iglesias, M. l.; Pellej, L.; Yum, J.-H.; González-Rodríguez, D.; Nazeeruddin, M. K.; Grätzel, M.; Clifford, J. N.; Palomares, E.; Vázqueza, P.; Torres, T. *Chem. Sci.* **2012**, *3*, 1177−1184.
(31) Anthonysamy, S.; Lee, Y.; Karunagaran, B.; Ganapathy, V.; Rhee, S.-W.; Karthikeyan, S.; Kim, K. S.; Ko, M. J.; Park, N.-G.; Ju, M.-J.; Kim, J. K. *J. Mater. Chem.* **2011**, *21*, 12389−12397.
(32) Lv, X.; Wang, F.; Li, Y. *ACS Appl. Mater. Interfaces* **2010**, *2*, 1980−1986.
(33) Griffith, M. J.; Sunahara, K.; Wagner, P.; Wagner, K.; Wallace, G. G.; Officer, D. L.; Furube, A.; Katoh, R.; Mori, S.; Mozer, A. J. *Chem. Commun.* **2012**, 4145−4162.
(34) Zeng, W.; Cao, Y.; Bai, Y.; Wang, Y.; Shi, Y.; Zhang, M.; Wang, F.; Pan, Y.; Wang, P. *Chem. Mater.* **2010**, *22*, 1915−1925.
(35) Shi, J.; Peng, S.; Pei, J.; Liang, Y.; Cheng, F.; Chen, J. *ACS Appl. Mater. Interfaces* **2009**, *1*, 944−950.
(36) Ying, W.; Guo, F.; Li, J.; Zhang, Q.; Wu, W.; Tian, H.; Hua, J. *ACS Appl. Mater. Interfaces* **2012**, *4*, 4215−4224.
(37) Abbotto, A.; Manfredi, N. *Dalton Trans.* **2011**, *40*, 12421−12438.
(38) Pavlishchuk, V. V.; Addison, A. W. *Inorg. Chim. Acta* **2000**, *298*, 97−102.
(39) Dai, F.-R.; Wu, W.-J.; Wang, Q.-W.; Tian, H.; Wong, W.-Y. *Dalton Trans.* **2011**, *40*, 2314−2323.
(40) Hagfeldt, A.; Grätzel, M. *Chem. Rev.* **1995**, *95*, 49−68.
(41) Hagfeldt, G.; Boschloo, L.; Sun, L.; Kloo, H.; Pettersson, H. *Chem. Rev.* **2010**, *110*, 6595−6663.
(42) Grätzel, M. *J. Photochem. Photobiol. C* **2003**, *4*, 145−153.
(43) Liang, M.; Lu, M.; Wang, Q.; Chen, W.; Han, H.; Sun, Z.; Xue, S. *J. Power Sources* **2011**, *196*, 1657−1664.
(44) Lu, M.; Liang, M.; Han, H.; Sun, Z.; Xue, S. *J. Phys. Chem. C* **2011**, *115*, 274−281.
(45) Zong, X. P.; Liang, M.; Fan, C. R.; Tang, K.; Li, G.; Sun, Z.; Xue, S. *J. Phys. Chem. C* **2012**, *116*, 11241−11250.
(46) Zong, X. P.; Liang, M.; Chen, T.; Jia, J. N.; Wang, L. N.; Sun, Z.; Xue, S. *Chem. Commun.* **2012**, *48*, 6645−6647.
(47) Han, L. Y.; Islam, A.; Chen, H.; Malapaka, C.; Chiranjeevi, B.; Zhang, S. F.; Yang, X. D.; Yanagida, M. *Energy Environ. Sci.* **2012**, *5*, 6057−6060.
(48) Ozawa, H.; Shimizu, R.; Arakawa, H. *RSC Adv.* **2012**, *2*, 3198−3200.
(49) Song, H. M.; Seo, K. D.; Kang, M. S.; Choi, I. T.; Kim, S. K.; Eom, Y. K.; Ryu, J. H.; Ju, M. J.; Kim, H. K. *J. Mater. Chem.* **2012**, *22*, 3786−3794.
(50) Holliman, P. J.; Mohsen, M.; Connell, A.; Davies, M. L.; Al-Salihi, K.; Pitak, M. B.; Tizzard, G. J.; Coles, S. J.; Harrington, R. W.; Clegg, W.; Serpa, C.; Fontes, O. H.; Charbonneaue, C.; Carnie, M. J. *J. Mater. Chem.* **2012**, *22*, 13318−13327.
(51) Cid, J. J.; Yum, J. H.; Jang, S. R.; Nazeeruddin, M. K.; Martinez-Ferrero, E.; Palomares, E.; Ko, J.; Grätzel, M.; Torres, T. *Angew. Chem., Int. Ed.* **2007**, *46*, 8358−8362.
(52) Yum, J.-H.; Jang, S.-R.; Walter, P.; Geiger, T.; Nüesch, F.; Kim, S.; Ko, J.; Grätzel, M.; Nazeeruddin, M. K. *Chem. Commun.* **2007**, 4680−4682.
(53) Fan, S.-Q.; Kim, C.; Fang, B. Z.; Liao, K.-X.; Yang, G.-J.; Li, C.-J.; Kim, J.-J.; Ko, J. *J. Phys. Chem. C* **2011**, *115*, 7747−7754.
(54) Neale, N. R.; Kopidakis, N.; Lagemaat, J. V. D.; Grätzel, M.; Frank, A. J. *J. Phys. Chem. B* **2005**, *109*, 23183−23189.
(55) Wang, Z.-S.; Cui, Y.; Dan-oh, Y.; Kasada, C.; Shinpo, A.; Hara, K. *J. Phys. Chem. C* **2007**, *111*, 7224−7230.
(56) Hao, X.; Liang, M.; Cheng, X.; Pian, X.; Sun, Z.; Xue, S. *Org. Lett.* **2011**, *13*, 5424−5427.
(57) Usami, A.; Seki, S.; Mita, Y.; Kobayashi, H.; Miyashiro, H.; Terada, N. *Sol. Energy Mater. Sol. Cells* **2009**, *93*, 840−842.
(58) Zhou, D.; Yu, Q.; Cai, N.; Bai, Y.; Wang, Y.; Wang, P. *Energy Environ. Sci.* **2011**, *4*, 2030−2034.
(59) Fabregat-Santiago, F.; Bisquert, J.; Garcia-Belmonte, G.; Boschloo, G.; Hagfeldt, A. *Sol. Energy Mater. Sol. Cells* **2005**, *87*, 117−131.
(60) Liang, Y.; Peng, B.; Chen, J. *J. Phys. Chem. C* **2010**, *114*, 10992−10998.
(61) Wang, Q.; Ito, S.; Grätzel, M.; Fabregat-Santiago, F.; Mora-Seró, I.; Bisquert, J.; Bessho, T.; Imai, H. *J. Phys. Chem. B* **2006**, *110*, 25210−25221.
(62) Bisquert, J.; Fabregat-Santiago, F.; Mora-Seró, I.; Garcia-Belmonte, G.; Gimenéz, S. *J. Phys. Chem. B* **2009**, *113*, 17278−17290.